View Article Online / Journal Homepage / Table of Contents for this issue
Dynamic Article Links

RSC Advances

Cite this: *RSC Advances*, 2012, **2**, 6295–6305

www.rsc.org/advances

PAPER

Supramolecular ionic strength-modulating microstructures and properties of nacre-like biomimetic nanocomposites containing high loading clay

Weijun Zhu,[ab] Chu-Hua Lu,[b] Feng-Chih Chang[b] and Shiao-Wei Kuo*[c]

Received 1st March 2012, Accepted 5th May 2012
DOI: 10.1039/c2ra20523h

Published on 09 May 2012. Downloaded on 28/04/2014 23:11:02.

In this study, we prepare thick nacre-like polymer clay nanocomposite films by a simple solution casting method. Nanoclay sheets with soft polymer coatings are used as ideal building blocks with intrinsic hard/soft character. The water-soluble poly(vinyl alcohol) (PVA) was chosen as an organic binder to connect each smectic clay sheet in the form of a nacre-like microstructure. The polymer-clay composite is in the form of a membrane in which the clay sheets are like stacked bricks. In addition, when applying normal stress larger than the yield stress—about 40 MPa—white shear bands develop at strains larger than 10%, much like the conditions where crazing of organic PVA is suppressed by inorganic fillers of clay sheets. Their corresponding microstructure and mechanical properties are studied using wide angle X-ray diffraction (WAXD), scanning electron microscopy (SEM), and transmission electron microscopy (TEM) techniques and a tensile testing machine and are discussed in detail.

Introduction

Nacre is an inorganic/organic composite material produced by some molluscs as an inner shell layer.[1] In this hybrid system, inorganic aragonite platelets, the crystal form of $CaCO_3$, are stacked orderly in the organic protein matrix. With a similar structure to a brick wall, this "brick-and-mortar" hierarchy contains high amounts of inorganic fillers,[2] in contrast to typical polymer composites which contain low amounts of inorganic components (< 20 wt.%).[3] The nacre-like microstructures inspired us to develop new inorganic/organic hybrid composites to satisfy the need of modern advanced materials, such as gas barrier membranes, electric insulation, flame-retardant building or furniture materials, the large-scale preparation of biomimetic materials is also of preeminent importance for future construction and coating applications.[4]

Recently, there have been some papers published regarding the preparation of nacre-like structures.[5] Smectic clays are the expected candidate of inorganic plate fillers because of their dimensions: one-nanometer thick and tens to hundreds of nanometers wide. Because of the polyionic character of clay, and their good dispersion and solubility in aqueous solutions; waterborne, water-soluble or water-dispersible polymers are chosen as the organic component. The selected clays must be well dispersed in water and the mixture should be a true solution in which the clay particles have a diameter of less than 100 nm. Otherwise clay aggregation in the opaque or the translucent solution could be left in the polymer matrix after water evaporation, resulting in opaque polymer/clay composites. Although clay is one of the oldest polymer composite materials, not all of them are suitable for nacre-like composites due to their different chemical structures. In view of these outstanding studies, Cloisite® Na^+ with the molecular formula of $Na_{0.75}[(Al_{3.25}Mg_{0.75})(Si_8O_{20})(OH)_4]$ and Laponite® RD[6] with the molecular formula of $Na_{0.7}[(Mg_{5.5}Li_{0.3})(Si_8O_{20})(OH)_4]$ have been used. These are the commercial brands of montmorillonite (MMT) and hectorite clays, respectively. Herein, sodium is an interlayer metal and aluminum, magnesium and lithium are intralayer metals, according to the sandwich-like structure of a clay molecule, as shown in Scheme 1. Both Cloisite® Na^+ and Laponite® RD readily dissolve in water.[7]

Compared to MMT, the Laponite® RD clay has intralayer Mg^{2+} instead of Al^{3+} and the low valence intralayer metals may make the layer packing weak and easy for water molecule penetration. In addition, the Laponite® clay in aqueous solution (< 0.03 g ml^{-1}) has circular disks of *ca.* 20–30 nm in diameter and a thickness *ca.* 1 nm, which meets the requirement of the size of inorganic fillers for a nacre-like inorganic/organic hybrid composite.[8] Cloisite® Na^+ MMT is a natural clay that 70–150 nm long.[9] Other MMT clays have not been used because they were not soluble enough in water. Besides materials, the chosen fabrication procedure could be the key step in the successful preparation of nacre-like microstructures. Four methods have been presented in the literature; including layer-by-layer assembly,[10] simple solution casting,[11] simple vacuum-filtration, and the doctor blade process.[12]

[a]*State Key Laboratory of Manufacturing Systems Engineering, Xi'an Jiaotong University, 710049 Xi'an, China*
[b]*Institute of Applied Chemistry, National Chiao Tung University, 30010 Hsinchu, Taiwan*
[c]*Department of Materials and Optoelectronic Science, National Sun Yat-Sen University, Kaohsiung, Taiwan. E-mail: kuosw@faculty.nsysu.edu.tw*

View Article Online

Published on 09 May 2012. Downloaded on 28/04/2014 23:11:02.

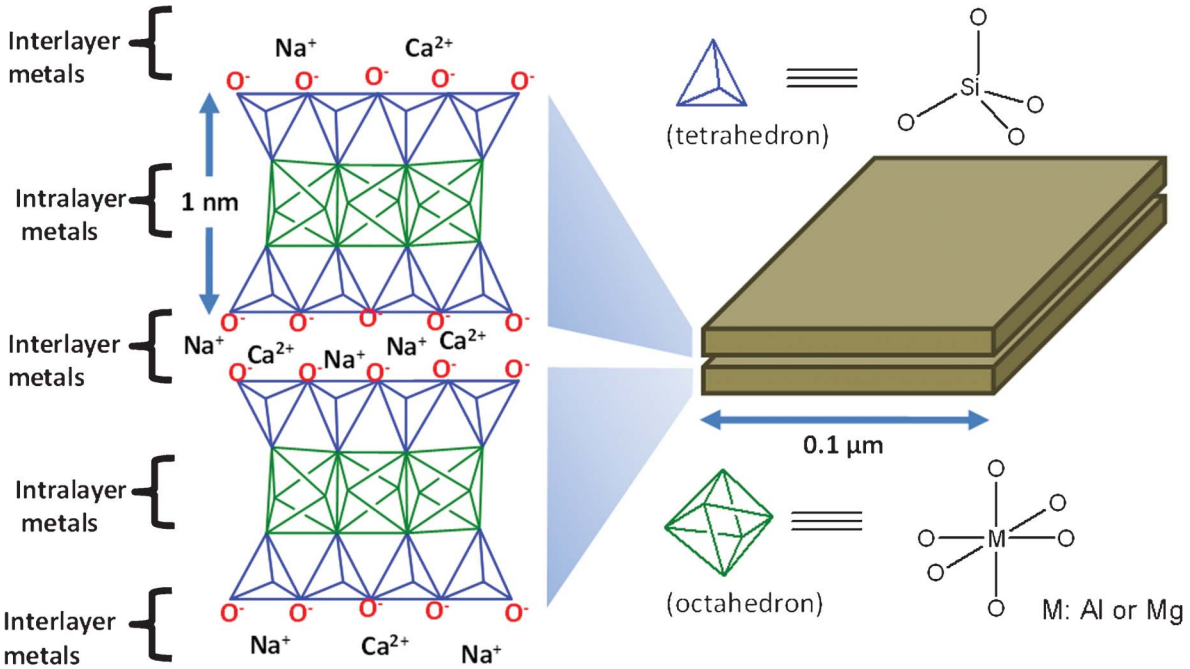

Scheme 1 Representation of layer-by-layer structures of clay microstructures.

Most MMT clays contain interlayer metals of Na^+ and Ca^{2+}. It is known that Ca^{2+} has a stronger ionic interaction with anionic silicate platelets than Na^+, making further modification difficult.[13] Furthermore, many organic MMT clays need to swell in water and require treating with a sodium source, such as NaOH, NaCl, $NaHCO_3$ before exchanging Na^+ with tertiary ammonium salts.[14] In most cases, it would be very easy to purify Na^+-MMT by centrifugal precipitation and washing with excess water to remove unwanted ions (such as ammonium, chloride, sulfate). However, it is still unclear whether collecting aggregate Na^+-MMT in the bottom of the container is the best method. Moreover, we believe that polyanionic aluminosilicate platelets can make stable dispersions in water *via* anionic repulsion if the chosen clay is treated appropriately. The dispersion of clay in water is a significant problem for polymer–clay nanocomposites, especially in the preparation of organic clays.

One of the commercial synthetic Na^+-MMTs was chosen for this study primarily because of its size, which was confirmed to be 50–100 nm by Lin *et al.*[14] Such a small raw material was key to producing a transparent nacre-like composite film and the transparency implies a microstructure without macroscopic aggregation. As described above, Ca^{2+} was removed by adding Na_2CO_3 because of the low water solubility of $CaCO_3$ side products. The clay dispersion was taken from the upper solution after separation by centrifugal force and the excess Na_2CO_3 was removed by dialysis. With so many steps for the preparation of a well-dispersed clay solution, we wondered if it was necessary to spend such extensive effort as treating Na^+-MMT with Na_2CO_3. This study had three clay solutions which were labeled samples A, B, and C, as shown in Scheme 2.

In addition to the dispersion of clay aqueous solutions, this study also focuses on the nacre-like clay polymer nanocomposite films, which are prepared by a simple solution casting method. The water-soluble poly(vinyl alcohol) (PVA) was chosen as a glue to connect each smectic clay sheet in the form of a nacre-like microstructure. The detailed microstructure and corresponding mechanical properties of the obtained composite films were examined by wide angle X-ray diffraction (WAXD), scanning electron microscopy (SEM), and transmission electron microscopy (TEM) techniques as well as a tensile testing machine.

Experimental section

Materials

PVA with a molecular weight of 95 000 g mol^{-1} and a hydrolysis ratio of 95% was supplied by ACROS Organics, Belgium. Synthetic sodium coordinated montmorillonite with a purity of more than 98% and a cation exchange coefficient (CEC) of 120 Meq 100 g^{-1} was purchased from Nanocor Inc. Sodium carbonate was obtained from SHOWA, Japan. Deionized water was used in all experiments.

Preparation of clay aqueous solution (A, B, and C)

As shown in Scheme 2, in the case of (a) without Na_2CO_3, 4 g of clay was mixed in 200 ml of water. The actual concentration of the mixture was 1.86 wt.%, determined by its dry weight and listed in Table 1. After ultrasonication at 40 °C for 1 day and then purification by centrifugation at 6000 rpm for 10 min, the upper layer was collected and labeled as Sample A with a concentration of 1.77 wt.% (Table 1). The leftover in the bottom was Sample SA gel, containing 25.78 wt.% dry clays. In the case of (b) with Na_2CO_3, but otherwise the same as case (a), the concentration of the original clay solution was found 2.63 wt.% because of the addition of 1.5 equimole of Na_2CO_3 based on the clay's CEC. After the same procedure, the upper layer was taken as Sample B with 2.58 wt.% dry clays and the leftover of Sample SB had 27.97 wt.% dry clays. After dialyzing Sample B against

 This journal is © The Royal Society of Chemistry 2012

View Article Online

Published on 09 May 2012. Downloaded on 28/04/2014 23:11:02.

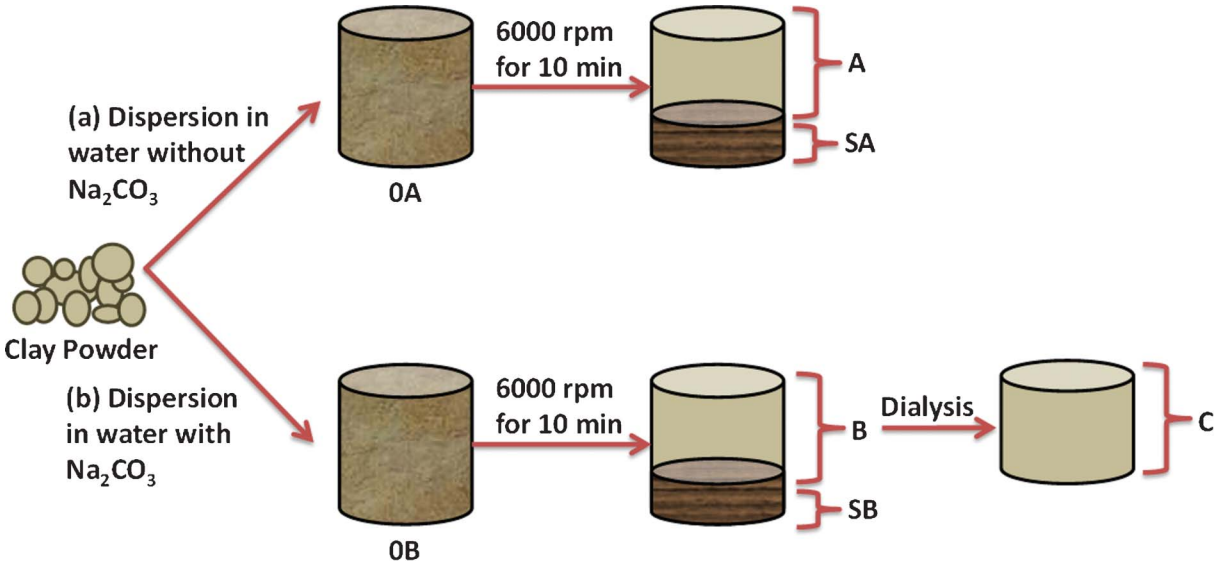

Scheme 2 Preparation procedure of clay aqueous solutions (a) without and (b) with Na_2CO_3, for samples 0A, A, SA, 0B, B, SB, and C.

Table 1 Concentration, zeta-potential and elemental ratios by EDS-assisted SEM with three probing places for each sample

Samples	Conc. (wt.%)	zeta-Potential (mV)[c]	Na/Si (×100)[e]	Ca/Si (×100)	Al/Si (×100)	Mg/Si (×100)
A	1.77[a]	−67.3	1.73 ± 0.17	0.34 ± 0.06	24.97 ± 0.14	1.57 ± 0.20
SA	25.78[a]	N.D.[d]	0.66 ± 0.14	1.50 ± 0.19	14.91 ± 0.91	0.63 ± 0.25
B	2.58[b]	N.D.	10.10 ± 3.49	N.D.	26.16 ± 0.54	1.45 ± 0.26
SB	27.97[b]	N.D.	2.08 ± 0.20	18.98 ± 4.54	15.49 ± 0.40	0.65 ± 0.12
C	1.53[b]	−60.1	1.46 ± 0.21	N.D.	25.50 ± 0.74	1.56 ± 0.18

[a] Original conc. = 1.86 wt.%. [b] Original conc. = 2.63 wt.% (contain Na_2CO_3). [c] Detected conc. =0.1 wt.%. [d] Non-detectable. [e] Arithmetic average ± standard deviation.

water, Sample C was obtained by removing excess salts, including Na_2CO_3 or other salts.

Preparation of clay–PVA nanocomposite films

The clay–PVA nanocomposites films were fabricated through solution casting after mixing Samples A, B, or C and 5 wt.% aqueous solutions of PVA according to the compositions listed in Table 1. Herein, the sample name of FP*X*Y refers to the composite films with added *X* wt.% of Sample Y clays in the dried weight. The well-dispersed mixtures were cast on a disposable plastic Petri dish and dried in an oven (25 °C; 70 RH%) for 2 days. Because of temporary aggregation where several nanoclay sheets were entangled in a PVA chain, the mixtures needed to be dispersed again by ultrasonication for 4 h before solution casting. Note that if the ultrasonication time was not enough to disperse the mixture, the resulting nanocomposites would turn into a little foggy as a result of large inhomogeneous aggregations.

Characterizations

Elemental ratios were characterized using scanning electron microscopy coupling with energy dispersive spectrometer (EDS-assisted SEM, Hitachi, S-4700I). Hydrodynamic diameters of clays in water were measured at particle concentrations listed in Table 1 using dynamic light scattering (DLS) with a Brookhaven 90 Plus particle analyzer equipped with a 655 nm laser. Ten runs of a one minute run duration were set for each measurement. The DLS size distribution was plotted using log-normal plots. The zeta potentials of the nanoparticles and aqueous clay solutions were measured using Malvern Zetasizer 3000HSA (Malvern Instruments, UK). The 0.1 wt.% clay solutions were diluted with deionized water and the zeta potentials were measured. UV-Vis spectra (DU700, Beckman) were used to characterize from 250 nm to 1050 nm. Inductively coupled plasma (ICP) elemental analysis measurements were carried out on a JY2000 Ultrace ICP Atomic Emission Spectrometer equipped with a JY AS 421 autosampler and 2400 g mm^{-1} holographic grating. X-ray diffraction (XRD) data were collected using the wiggler beamline BL17A1 of the National Synchrotron Radiation Research Center (NSRRC), Taiwan. A triangular bent Si (111) single crystal was employed to obtain a monochromated beam with a wavelength (λ) of 1.33001 Å. The XRD patterns were collected using an imaging plate (IP; Fuji BAS III; area = 20 × 40 cm^2) curved with a radius equivalent to the sample-to-detector distance (280 mm). The two-dimensional (2D) XRD patterns observed for the sample (typical diameter: 10 mm; thickness: 1 mm) were circularly averaged to obtain a one-dimensional (1D) diffraction profile $I(Q)$. TEM images were recorded using a JEOL-2100 transmission electron microscope operated at an accelerating voltage of 200 kV. Ultrathin sections of the TEM samples were prepared using a Leica Ultracut UCT microtome. The tensile properties were measured according to ASTM 638 on a Shimadzu AG-50kNE universal tester. The crosshead speed was set at 1 mm min^{-1}.

View Article Online

Published on 09 May 2012. Downloaded on 28/04/2014 23:11:02.

Results and discussion

Dispersion of clay aqueous solutions

As shown in Fig. 1, in both cases of (a) without Na_2CO_3 and (b) with Na_2CO_3, the original dispersions (Samples 0A and 0B) look muddy and have particles suspended in them. After centrifugal separation, Sample A turned clear by precipitating large clay particles (Sample SA). Because of the presence of Na_2CO_3, Sample B remained cloudy and Sample C became clear after dialyzing Sample B against water. Compared to the previous studies,[15] this study prolonged the time of ultrasonic dispersion to 1 day to separate the stacked smectic clay sheets in water, resulting in a delaminated phase of Na^+-montmorillonite with a "house-of-cards" structure.[16] Furthermore, in our view after centrifugal separation[17] the dispersed clay solution should have been stable for several weeks. Note that using different sources of clays could have different results depending on their sizes, composition, structure, and procedures. Even though EDS-assisted SEM has relatively low precision of elemental analyses, the results could also provide useful information.

As presented in Table 1, the centrifugal separation is also an appropriate method to remove unwanted Ca^{2+}, when comparing Ca/Al ratios of 0.34 (Sample A) with 1.50 (Sample SA). Moreover, Samples A and B had more Mg^{2+} than Samples SA and SB, implying that the composition plays an important role in the dispersion of clay solutions. This observation is consistent with the characteristic of water-dispersible Laponite® RD with the chemical formula of $Na_{0.7}[(Mg_{5.5}Li_{0.3})(Si_8O_{20})(OH)_4]$.

Also from Table 1, the addition of Na_2CO_3 would help Ca^{2+} sedimentation in the form of $CaCO_3$ for increasing the Sample SB elemental ratio of Ca^{2+} to Si by more than one order of magnitude. However, the dialysis was necessary to get rid of excess Na_2CO_3. The relatively large errors of $\pm$ 3.49 and $\pm$ 4.54 in Samples B and SB resulted from inhomogeneous Na_2CO_3 and $CaCO_3$ crystal particles scattered in the detected areas. With the treatment, the Na^+ content was the largest in Sample B, and the smallest in Sample C. Three samples A, B, and C were used to blend with PVA solution for the preparation of clay–PVA nanocomposite films with different Na^+ contents.

In addition to the composition, the size of the clay particles in water also determined the appearance of the solutions. In Fig. 2, DLS spectra have three results to show the size distribution of clay nanoparticles in water. For these three Samples, 0A, A, and C, the curves of the correlation functions are smooth and converge on the base lines, representing reliable signals of light scattering on the clay particles in water. Comparing Fig. 2-a and 2-b, we find that the large clay particles with a mean diameter of 3.3 μm have been precipitated by centrifugal separation at

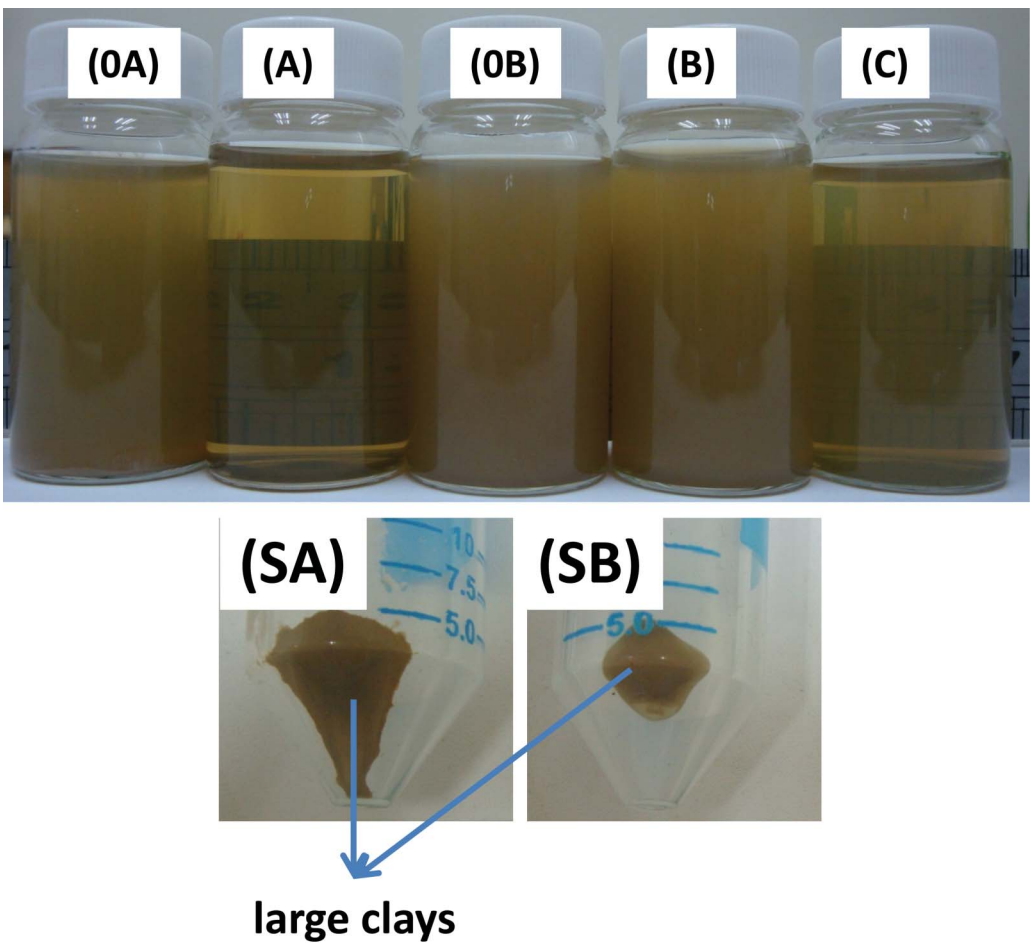

Fig. 1 Photographs of clay solutions: pristine (0A) without Na_2CO_3, pristine (0B) with Na_2CO_3, upper layer of (A and B) after centrifugal separation of 0A and 0B, the leftovers of SA and SB, and (C) after dialysis of B.

 This journal is © The Royal Society of Chemistry 2012

View Article Online

Published on 09 May 2012. Downloaded on 28/04/2014 23:11:02.

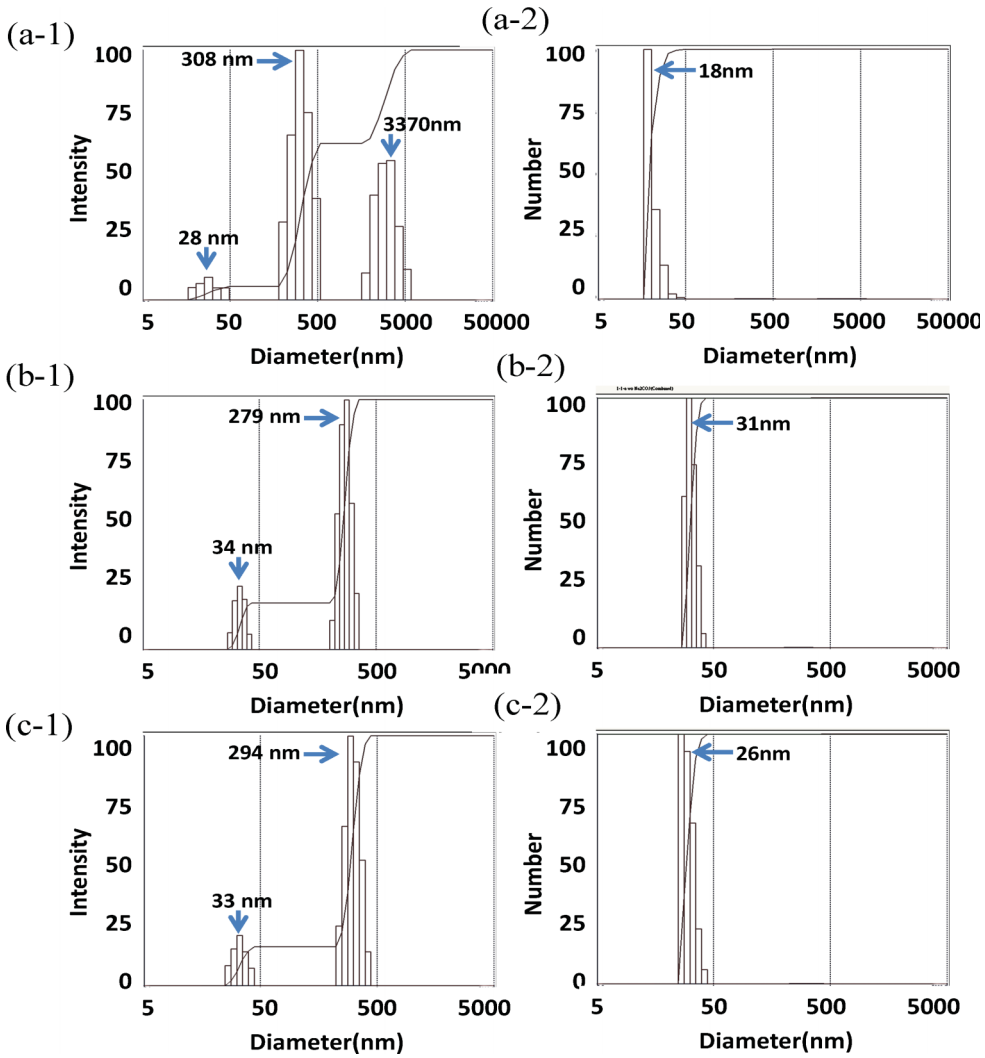

Fig. 2 DLS results of Sample A (a) before and (b) after centrifugal separation and Sample B (c) after centrifugal separation with three models of 1: intensity and 2: number.

6000 rpm for 10 min, according to the clearer solution of Sample A in Fig. 1. As explained by mathematical models, the discrepancy between intensity and number arises from the fact that large particles scatter much more light than small particles (the intensity of scattering of a particle is proportional to the sixth power of its diameter (from Rayleigh's approximation).[18] Then, by this separation method, the average size of most clay nanoparticles was found to be 31 nm and a small quantity of them had a mean diameter of 279 nm. The latter seems imperfect but a commercial product of clays with small defects is good enough for further study. By treating with Na_2CO_3, Sample C had similar results to Sample A. Moreover, as listed in Table 1, the zeta potentials of −67.3 and −60.1 mV for Samples A and C were less than that of Na^+-Cloisite (−28 mV) and Laponite (−60 mV), indicating stronger ionic repulsion between clay sheets for more stable colloidal solution.[19] Lin *et al.* have investigated the particle size of this commercial clay by TEM technique and DLS analysis. In their study, the size of the pristine sodium montmorillonite (Na^+-MMT) was about 700–850 nm in water after treatment with poly(oxyethylene)diamine the size of the modified MMT reduced to 50–100 nm.[20] In contrast, this study proved that a pure aqueous solution of separate clay sheets can be prepared by ultrasonic dispersion and centrifugal purification. Lin *et al.* also showed that the zeta potential of Na^+-MMT is about −20 mV at pH 7, whose absolute value is lower than our results of −67.3 and −60.1 mV for Samples A and C, respectively.[20]

The significance of the zeta potential is that its value can be related to the stability of the colloidal dispersions. The zeta potential indicates the degree of repulsion between adjacent, similarly charged particles in dispersion. For molecules and particles that are small enough, a high zeta potential will confer stability, *i.e.*, the solution or dispersion will resist aggregation.[21]

Investigated by DLS and zeta potential, the clay solutions in this study was suitable for the preparation of nacre-like composites. The clay materials chosen for the preparation of nacre-like composites should not be limited to Laponite® RD, Cloisite® Na^+, or other special clays. The important concept shown in this study is that the appropriate clay materials need to consider the size, composition, and preparation method.

View Article Online

Published on 09 May 2012. Downloaded on 28/04/2014 23:11:02.

Fabrication of clay–PVA Nanocomposite films

The well dispersed aqueous clay solutions are crucial to obtain optically transparent composite films after mixing with water-soluble polymers. There are three kinds of water-based polymer systems: water-soluble, waterborne, and water-dispersed. All of the repeating units of a water-soluble polymer are water soluble while in a waterborne polymer, only parts of the polymer chains are hydrophilic. A water-dispersed polymer needs a surfactant to help the dispersion of the hydrophobic chains in water. Like most references,[6,10–11,22] in this study, a water-soluble PVA was chosen as an organic binder to fabricate clay–polymer composites in the form of a membrane in which clay sheets are in the form of stacked bricks.

When two clear clay and PVA solutions are mixed, the formation of small and large aggregates leads to an opaque mixture, as shown in Scheme 3. This phase change results from the fact that while partial PVA repeating units connect with clay sheets *via* a hydrogen bond (O–H/O–), the connection points become hydrophobic because of the lack of active sites with water molecules.[23] However, the prolonged treatment of ultrasonication can dissociate transient and large aggregates into stable and small ones. In the drying process, the solutions of clay–PVA composites first turn into a gel and then gradually become clear while most of the water evaporated in an oven.[14] In the final step of forming a dry membrane, the "house-of-cards" structure of clay network gel would collapse and stack into a pile of clay sheets.[6] Considering Sample C as an example, the photograph in Fig. 3-a shows the transparent and flexible composite films of FP55C with an average 30 μm thickness containing 55 wt.%

Sample C clay. Herein FP*X*Y refers to the composite films adding *X* wt.% of Sample Y clays in the dried weight. For more details, this study provides UV-vis results, but the absorbencies of these different thickness composite films are difficult to compare.[23]

According to the Beer–Lambert law of $A = \varepsilon bc$,[24] where ε and c are the extinction coefficient and concentration of absorbing species, respectively, and b is the path length through the material. Absorbance (A) was normalized by the thickness of the composite films, which results in the absorption coefficient (εc) of the substance. Herein, the absorption coefficient is useful for predicting the optical loss of composite films at a given wavelength and thickness. In Fig. 3b, this study observes the higher absorbance coefficient of FP90C and FP100C within the visible light wavelengths from 400 nm to 800 nm, resulting in the opaque appearance. A possible reason is that the presence of so many clay sheets in a small volume makes stacking in parallel more difficult, resulting in large aggregations which scatter visible light.[23] In other words, the more organic parts covered the periphery of clay sheets render the space for them to stack more orderly into the layer-by-layer structure. In addition, the intrinsic absorbance of separate clay sheet at 244 nm tends to extend to 600 nm, arising from the clays containing Fe ions. This effect would be more significant with the increase of clay contents, showing transparent and dark yellow appearances.

Microstructures of clay–PVA nanocomposite films

As in other studies on clay–polymer nanocomposites,[23] we used X-ray diffraction to detect the organic gap width between two adjacent clay sheets. For early studies where the amount of inorganic clay was less than 20 wt.%, the dispersion of clay sheets can be classified into intercalation and exfoliation, depending on whether *d*-spacing distance between two adjacent clay sheets is observed or not. In this case, the stacking between clay sheets is inevitable because the volume fraction of the inorganic component is significant increased and exfoliated dispersion of

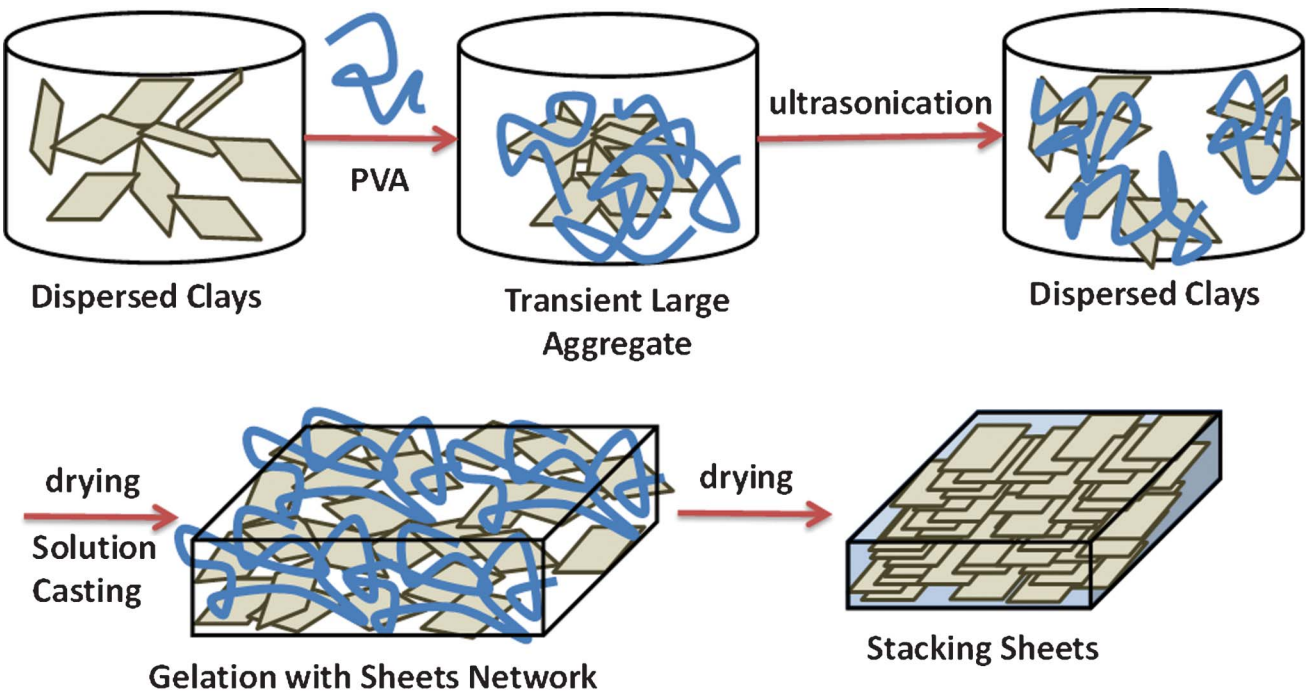

Scheme 3 Representation of the process of solution casting to fabricate nacre-like microstructures.

 This journal is © The Royal Society of Chemistry 2012

Published on 09 May 2012. Downloaded on 28/04/2014 23:11:02.

the clay sheets is almost impossible. For composites with high inorganic content, our major concerns were the method to fabricate an ordered layer-by-layer structure and the relevant microstructures and performances. As shown in Fig. 4a, the first peak of stacked clay sheet was observed when the clay content of clay–PVA nanocomposites was more than 30 wt.%. In other words, the exfoliated clay sheets can be well dispersed in the PVA medium as long as the volume fraction of inorganic fillers is not higher than 30 wt.%. With increasing the amount of inorganic clays, the first peak of stacked clay sheets would shift into higher diffraction angles. According to Bragg's law of $n\lambda = 2d\sin\theta$, where n equals 1 for major diffraction, λ is the wavelength of incident wave, d is the spacing between planes, and θ is the angle between the incident ray and the scattering planes. The d-spacing distance of the first peak of the stacked clay structure in Fig. 4b linearly decays along with the increase of clay contents, indicating that PVA chains not only wrap each clay sheet well but also make PVA-covered sheets well dispersed in the system. The data in Fig. 3 and 4 indicated that 50 wt.% of clay content would be the best choice for a transparent clay–PVA nanocomposite film with a nacre-like microstructure. In this case, the PVA component is more than the amount necessary to cover each clay sheet and to render room to stack the clay sheets regularly.

Fig. 5a shows the 2D XRD patterns of the FP50C film. As expected, there is no signal in the through-plane view for a layer-by-layer microstructure and in contrast, this study has at least three order signals in the in-plane view. These three peaks in the 1D XRD curve respond to a group of d-spacing distances (2θ) of 2.88 nm (3.06°), 1.46 nm (6.04°), and 0.95 nm (9.35°), respectively. These three peaks are identical to those shown in Fig. 4a by the reflective XRD. This result is different from the

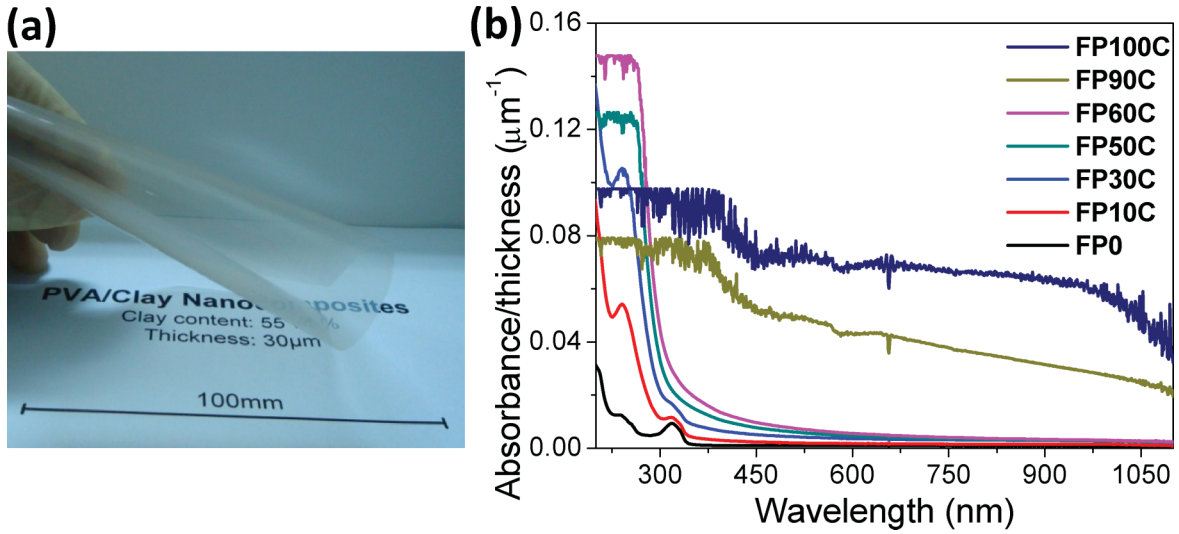

Fig. 3 (a) Photograph of a FP55C film, and (b) UV-vis spectra of FPXY. Herein FPXY refers to the composite films with X wt.% of Sample Y clays in the dried weight. (From top to down indicating 100 to 0 wt.%).

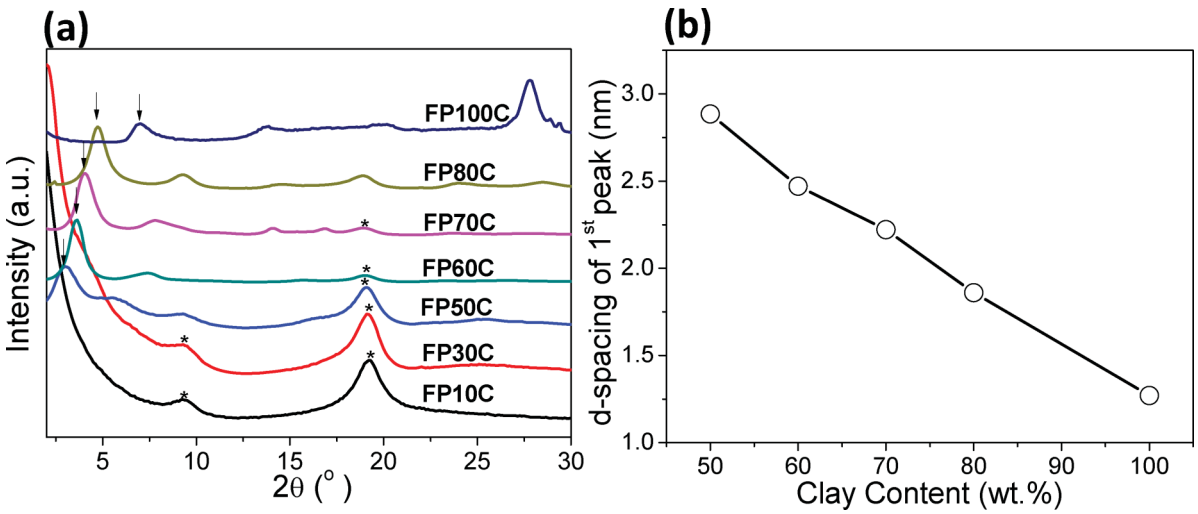

Fig. 4 (a) XRD spectra and (b) the d-spacing distances of FPXY. Herein FPXY refers to the composite films containing X wt.% of Sample Y clays in dried weight and the asterisk and arrow marks indicate the signals of pure PVA and the first peak of stacked clay sheets, respectively.

View Article Online

Published on 09 May 2012. Downloaded on 28/04/2014 23:11:02.

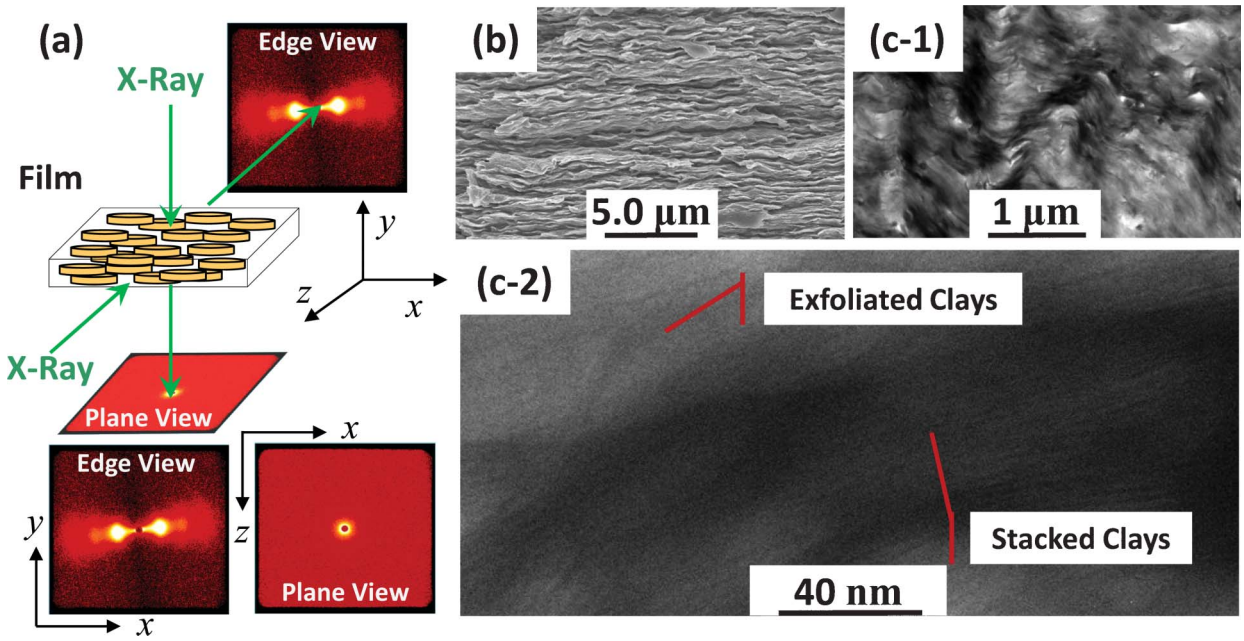

Fig. 5 (a) 2D XRD patterns, (b) SEM image, and (c) TEM images of FP50C.

results presented by Koo *et al.*[25] In their study, Koo *et al.* attribute second small angle X-ray scattering (SAXS) signals produced from the X-ray scattering to the aggregation of the organic clays.

In addition to the spectral analyses, we also used SEM and TEM techniques to confirm the layer-by-layer structure in a small domain. In Fig. 5b, the SEM image shows the layer stacked microstructure in the cross-section of the fractured film. The ragged topology results from the relative motion between flexible PVA chains and rigid clay sheets. The TEM image in Fig. 5c shows the dark distribution of microtomed inorganic clay sheets. At the higher magnification in Fig. 5c-2, the TEM image indicated ~3 nm gaps between layers corresponding to the XRD or the SAXS results.

Mechanical properties of clay–PVA nanocomposite films

In this study we were also interested in the mechanical performance of nacre-like clay–PVA nanocomposite films. Fig. 6a shows the real time observation during a tensile test of a FP50C membrane as an example. Before extension, the film was so transparent that the clamp fastener behind it was visible.

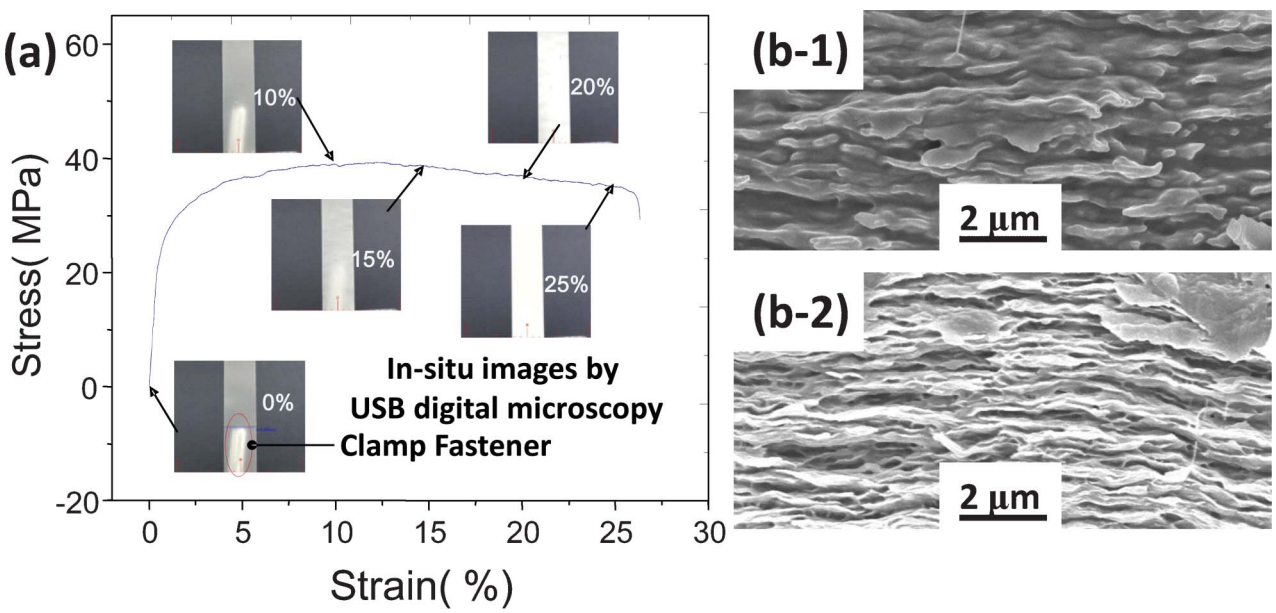

Fig. 6 (a) Stress-strain curve and *in situ* images of FP50C composite membranes in a tensile test and (b) SEM cross sectional images, before (b-1) and after (b-2) the tensile test.

 This journal is © The Royal Society of Chemistry 2012

View Article Online

Published on 09 May 2012. Downloaded on 28/04/2014 23:11:02.

Table 2 Elemental ratios examined by ICP-AES

Samples	Na/Al (× 100)	Ca/Al (× 100)	Mg/Al (× 100)
A	28.69	1.77	14.05
B	109.42	0.50	13.76
C	19.51	0.28	13.53

While stretching the specimen, the width remained almost the same. Applying normal stress larger than the yield stress—about 40 MPa—white shear bands develop at strains larger than 10%, much like the conditions where crazing of organic PVA is suppressed by inorganic fillers of clay sheets. The SEM micrographs in Fig. 6b indicate that during extension, parts of organic PVA were drawn out of regions between clay sheets, and then clay sheets were forced to shift in the longitudinal direction because they are joined by strong hydrogen bonds between Si–O–Si and the O–H groups of PVA.[26] In addition, the inorganic fillers of clay sheets tend to restrain specimen shrinkage in the longitudinal direction. Therefore, the remaining vacancies not only make the microstructure more ragged in Fig. 6b-2 but also induce a white appearance because of the visible light scattering on it. This phenomenon could be used to explain the nacre structure-induced mechanical reinforcement of the clay–polymer composites.

According to the procedure of FP50C preparation, FP50A and FP50B are similar clay–PVA composite films with the same clay content of 50 wt.%. These were compared to determine the

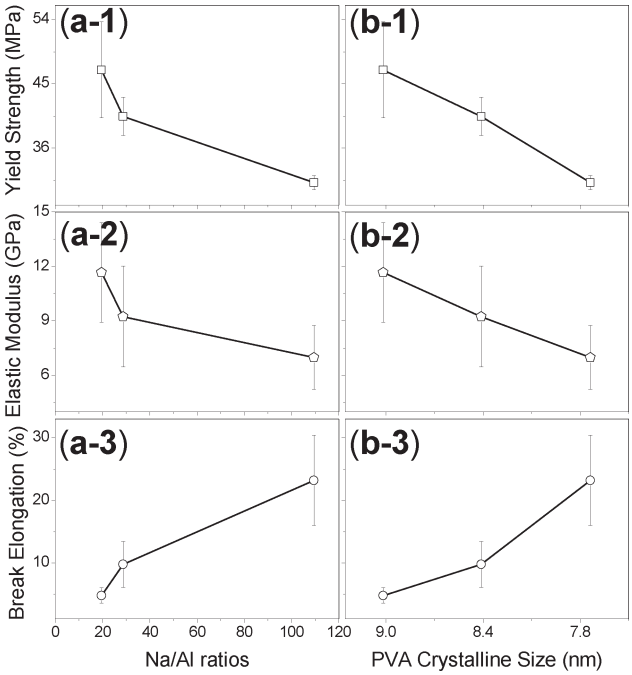

Fig. 8 Relationships between mechanical properties and (a) Na/Al ratios and (b) PVA crystalline size, including: 1. yield strength, 2. elastic modulus, and 3. break elongation.

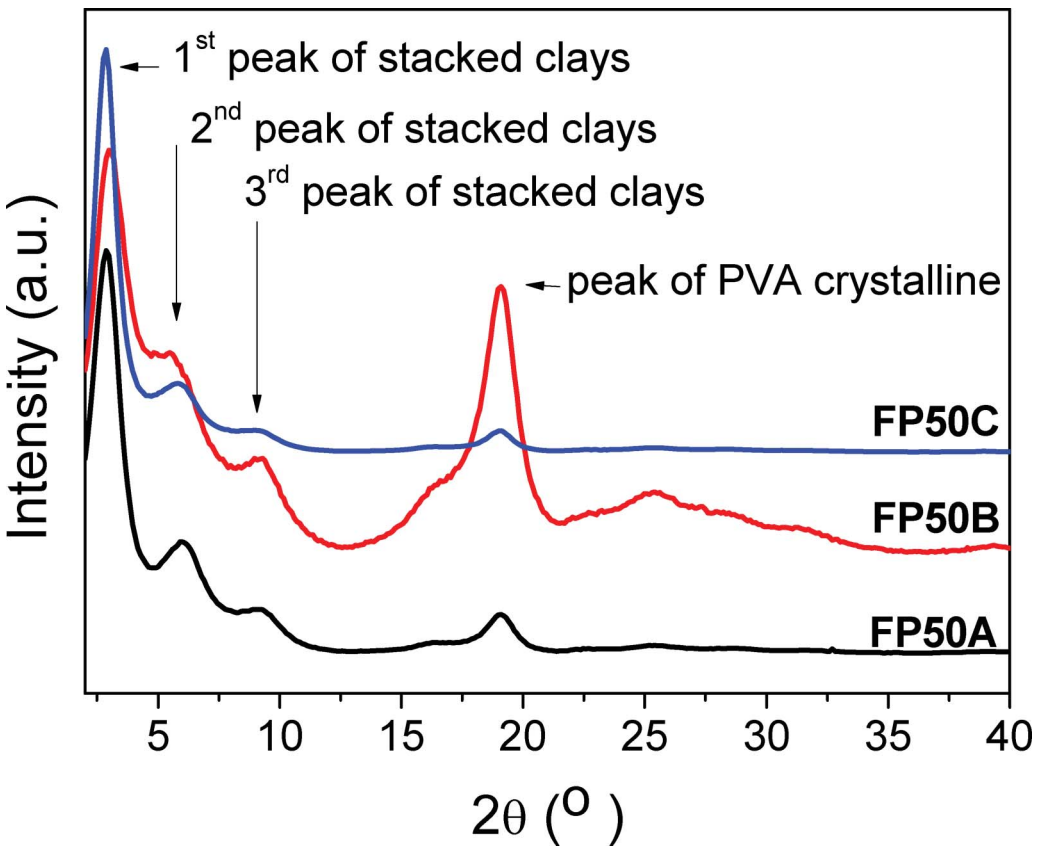

Fig. 7 XRD spectra of (a) FP50A, (b) FP50B, and (c) FP50C.

View Article Online

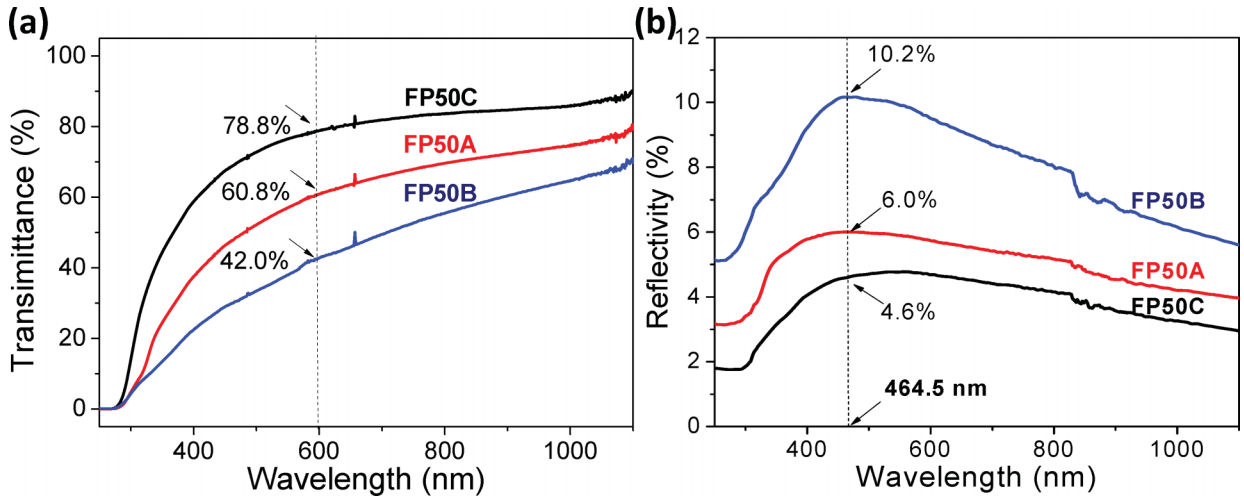

Fig. 9 Transmittance and reflectivity of FP50A, FP50B, and FP50C.

Published on 09 May 2012. Downloaded on 28/04/2014 23:11:02.

effect of salt content on the mechanical properties of clay–PVA nanocomposite films. As presented in Table 2, the more accurate elemental composition of Samples A, B, and C were measured by inductively coupled plasma atomic emission spectrometry (ICP-AES). The element distribution and surface roughness of the specimens have strongly affected the accuracy of the EDS results. However, Samples SA and SB were soluble in water and it was worth analyzing them to understand the composition effect on the dispersion of clay solutions by EDS elemental analysis. The elemental analysis by ICP-AES is necessary for discussions on the quantitative results. In Table 1, the elemental ratios of Al to Si are almost the same for Samples A, B, and C. Considering Al as the base element is helpful to show the compositions with higher signal-to-noise ratios. After treatment with Na_2CO_3, the elemental ratio of sodium to aluminum was as high as 109.42 for Sample B and after dialysis against water, it reduced to 19.51 for Sample C, which is less than the 28.69 of Sample A. In this study we normalized the signal of the first peak in the stacking clay sheets and found that the sodium content had a strong tendency to induce heterogeneous crystallization of free PVA domains, resulting in the greater intensity of highly crystalline FP50B compared to FP50A and FP50C, as shown in Fig. 7. According to Scherrer's equation of $d_{hkl} = 0.9\lambda/(B\cos\theta)$, the peak width ($B$) can be used to calculate the average size (d_{hkl}) of PVA crystal domains regarded as physical linking points to reinforce the mechanical properties of the composite membranes, where λ is the X-ray wavelength and θ is the Bragg angle.[27] Fig. 8 shows that the higher sodium content could induce a smaller and denser PVA crystalline domain. Although the data has a high standard deviation, it clearly shows a strong effect on the mechanical properties, especially yield strength and elastic modulus

Optical properties of clay–PVA nanocomposite films

Besides mechanical properties, we also studied the effect of the salt content on the optical properties of the composite membranes. The transparent appearance of some composite membranes is an interesting phenomenon because it would be necessary to keep the size of phase separation smaller than 100 nm to prevent visible light scattering on these membranes. Including this study, only a few research efforts have successfully prepared such transparent composite films with a clay content higher than 50 wt.%.[7,22b]

As shown in Fig. 9, the salt content has a great effect on the transmittance and reflectivity of the clay–PVA composite films. The data show that transmittances at 600 nm are 60.8%, 78.8%, and 42.0% and the reflectivities at 464.5 nm are 6.0%, 4.6%, and 10.2% for FP50A, FP50B, and FP50C samples, respectively. In Fig. 7, all three membranes showed three strong peaks for the stacked clay sheets but these peaks indicate that the stacking behaviour happens on the several nanometer dimension scale. Therefore, this study supposed that the long-ranged order could be poor with the large content of Na_2CO_3 and the more clay sheets in a domain would induce higher absorbance, resulting in low transmittance and high reflectivity of FP50B.

Conclusions

Unlike the random and exfoliated distribution of inorganic sheets in the low inorganic content of polymer nanocomposites, the exfoliated clay sheets can be well dispersed in the PVA medium as long as the volume fraction of inorganic fillers is not larger than 30 wt.%. However, the clay sheets tend to stack parallel with the high inorganic content when clay contents are larger than 30 wt.%. In this study, the polymer clay composites based on PVA with nacre-like structures were successfully prepared. This enables us to tailor and strengthen the mechanical properties on demand and possibly in a patterned fashion by the supramolecular structure.

Acknowledgements

This work was supported financially by the National Science Council, Taiwan, Republic of China, under Contracts No. NSC 100-2221-E-110-029-MY3 and NSC 100-2628-E-110-001.

References

1 (*a*) A. H. Heuer, D. J. Fink, V. J. Laraia, J. L. Arias, P. D. Calvert, K. Kendall, G. L. Messing, J. Blackwell, P. C. Rieke, D. H. Thompson, A. P. Wheeler, A. Veis and A. I. Caplan, *Science*, 1992, **255**, 1098; (*b*) L. Addadi and S. Weiner, *Nature*, 1997, **389**, 912.

 This journal is © The Royal Society of Chemistry 2012

View Article Online

2 (*a*) G. Mayer, *Science*, 2005, **310**, 1144; (*b*) H. D. Espinosa, J. E. Rim, F. Barthelat and M. J. Buehler, *Prog. Mater. Sci.*, 2009, **54**, 1059.
3 (*a*) R. Gangopadhyay and A. De, *Chem. Mater.*, 2000, **12**, 608; (*b*) H. K. Fu, C. F. Huang, S. W. Kuo, H. C. Lin, D. R. Yei and F. C. Chang, *Macromol. Rapid Commun.*, 2008, **29**, 1216; (*c*) X. Fu and Q. Qutabuddin, *Polymer*, 2001, **42**, 807.
4 (*a*) C. Sanchez, P. Belleville, M. Popall and L. Nicole, *Chem. Soc. Rev.*, 2011, **40**, 696; (*b*) F. Gao, *Mater. Today*, 2004, **7**, 50; (*c*) P. Kiliaris and C. D. Papaspyrides, *Prog. Polym. Sci.*, 2010, **35**, 902; (*d*) A. Walther, I. Bjurhager, J. M. Malho, J. Ruokolainen, L. Berglund and O. Ikkala, *Angew. Chem., Int. Ed.*, 2010, **49**, 6448.
5 (*a*) E. A. Stefanescu, C. Stefanescu, I. I. Negulescu and W. H. Daly, *Macromol. Chem. Phys.*, 2008, **209**, 2320; (*b*) K. Shikinaka, K. Aizawa, N. Fujii, Y. Osada, M. Tokita, J. Watanabe and K. Shigehara, *Langmuir*, 2010, **26**, 12493; (*c*) K. E. Strawhecker and E. Manias, *Chem. Mater.*, 2000, **12**, 2943; (*d*) T. Ebina and F. Mizukami, *Adv. Mater.*, 2007, **19**, 2450; (*e*) X. Zhao, Q. Zhang, Y. Hao, Y. Li, Y. Fang and D. Chen, *Macromolecules*, 2010, **43**, 9411; (*f*) A. K. Kaushik, P. Podsiadlo, M. Qin, C. M. Shaw, A. M. Waas, N. A. Kotov and E. M. Arruda, *Macromolecules*, 2009, **42**, 6588.
6 E. A. Stefanescu, C. Stefanescu, B. C. Donose, J. C. Garon, W. H. Daly, G. Schmidt and I. I. Negulescu, *Macromol. Mater. Eng.*, 2008, **293**, 771.
7 P. Podsiadlo, A. K. Kaushik, E. M. Arruda, A. M. Waas, B. S. Shim, J. D. Xu, H. Nandivada, B. G. Pumplin, J. Lahann, A. Ramamoorthy and N. A. Kotov, *Science*, 2007, **318**, 80.
8 R. Avery and J. Ramsay, *J. Colloid Interface Sci.*, 1986, **109**, 448.
9 K. Kim, J. H. Kim and I. J. Chung, *J. Appl. Polym. Sci.*, 2011, **119**, 1287.
10 A. Liu, A. Walther, O. Ikkala, L. Belova and L. A. Berglund, *Biomacromolecules*, 2011, **12**, 633.
11 T. Ebina and F. Mizukami, *Adv. Mater.*, 2007, **19**, 2450.
12 A. Walther, I. Bjurhager, J. M. Malho, J. Pere, J. Ruokolainen, L. A. Berglund and O. Ikkala, *Nano Lett.*, 2010, **10**, 2742.
13 R. C. Zielke and T. J. Pinnavai, *Clays Clay Miner.*, 1988, **36**, 403.
14 J. J. Lin, C. C. Chu, C. C. Chou and F. S. Shieu, *Adv. Mater.*, 2005, **17**, 301.
15 (*a*) S. P. Katdare, V. Ramaswamy and A. V. Ramaswamy, *Catal. Today*, 1999, **49**, 313; (*b*) S. P. Katdare, V. Ramaswamy and A. V. Ramaswamy, *J. Mater. Chem.*, 1997, **7**, 2197.
16 T. J. Pinnavia, M. S. Tzou, S. D. Landau and R. H. Raythatha, *J. Mol. Catal.*, 1984, **27**, 195.
17 D. C. Bush, R. E. Jenkins and S. B. McCaleb, *Clays Clay Miner.*, 1996, **14**, 407.
18 J. Doak, R. K. Gupta, K. Manivannan, K. Ghosh and P. K. Kahol, *Phys. E.*, 2010, **42**, 1605.
19 (*a*) E. Bretsnajdrova, L. Svoboda and J. J. Zelenka, *Journal of Electrical Engineering*, 2010, **61**, 302; (*b*) S. Zhang, Q. Lan, Q. Liu, J. Xu and D. C. Sun, *Colloids Surf., A*, 2008, **317**, 406.
20 J. J. Lin, C. C. Chu, M. L. Chiang and W. C. Tsai, *J. Phys. Chem. B*, 2006, **110**, 18115.
21 A. K. Atmuri, S. R. Bhatia and A. F. Routh, *Langmuir*, 2012, **28**, 2652.
22 (*a*) B. Long, C. A. Wang, W. Lin, Y. Huang and J. Sun, *Compos. Sci. Technol.*, 2007, **67**, 2770; (*b*) S. Srivastava and N. A. Kotov, *Acc. Chem. Res.*, 2008, **41**, 1831; (*c*) H. B. Yao, Z. H. Tan, H. Y. Fang and S. H. Yu, *Angew. Chem., Int. Ed.*, 2010, **49**, 10127.
23 (*a*) E. Loizou, P. Butler, L. Porcar, E. Kesselman, Y. Talmon, A. Dundigalla and G. Schmit, *Macromolecules*, 2005, **38**, 2047; (*b*) E. Paineau, I. Bihannic, C. Baravian, A. M. Philippe, P. Davidson, P. Levitz, S. S. Funari, C. Rochas and L. J. Michot, *Langmuir*, 2011, **27**, 5562; (*c*) E. Paineau, L. J. Michot, I. Bihannic and C. Baravian, *Langmuir*, 2011, **27**, 7806.
24 J. D. J. Ingle, S. R. Crouch, *Spectrochemical Analysis*, Prentice Hall, New Jersey, 1988.
25 C. M. Koo, H. T. Ham, S. Q. Kim, K. H. Wang and I. J. Chung, *Macromolecules*, 2002, **35**, 5116.
26 (*a*) S. W. Kuo and F. C. Chang, *Prog. Polym. Sci.*, 2011, **36**, 1649; (*b*) Y. J. Lee, S. W. Kuo, W. J. Huang, H. Y. Lee and F. C. Chang, *J. Polym. Sci., Part B: Polym. Phys.*, 2004, **42**, 1127.
27 B. D. Cullity, S. R. Stock, *Elements of X-Ray Diffraction, 3rd Ed.*, Prentice-Hall Inc., 2001.

Published on 09 May 2012. Downloaded on 28/04/2014 23:11:02.